Supporting Information

Dense CO Adlayers as Enablers of CO Hydrogenation on Ru-Based Catalysts

Jianwei Liu[a,b], David Hibbitts*[,b,c] and Enrique Iglesia*[,b]

[a]State Key Laboratory of Heavy Oil Processing, China University of Petroleum, Qingdao, 266580, China

[b]Department of Chemical and Biomolecular Engineering, University of California, Berkeley, California, 94720, United States

[c]Department of Chemical Engineering, University of Florida, Gainesville, Florida, 32611, United States

*Corresponding author: Fax: + 1 510 642 4778

Email address: hibbitts@ufl.edu (D. Hibbitts), iglesia@berkeley.edu (E. Iglesia)

S1. Elimination of heat- and mass-transfer effects during CO hydrogenation

Both heat and mass transport limitations should be rigorously excluded because of their ubiquitous strong effects on measured rates as a result of the very exothermic nature of the CO hydrogenation reaction and of the inverse dependence of rates on the concentration of CO, the likely diffusion-limited reactant. Many discrepancies among reported FTS and methanation turnover rates are likely to reflect prevalent gradients that have gone unrecognized and unmitigated, thus corrupting measurements of reactivity and even of the form of the rate equations. CO hydrogenation turnover rates at steady state conditions on catalysts with different intraparticle and interparticle dilution ratios (1:5 to 1:50 and 1:20 to 1:100, respectively; 5% wt. Ru/SiO_2, 7.5 nm particle size; 573K, 2 kPa CO, 60 kPa H_2, and 8 kPa H_2O) are of invariance (Fig. S1), suggesting the absence of both heat and mass transport limitations at the conditions used in this study and that changes in rate solely reflect changes in kinetic behavior. Strict absence of both heat and mass transport limitations are achieved by intraparticle and interparticle dilution of the catalysts as described in Section 2.3.

CO hydrogenation turnover rates decrease with time on stream (Fig. S1) for all samples, indicating that catalysts deactivate slowly during the reaction. All the rates reported herein are corrected by periodic rate measurements at a reference condition (2 kPa CO, 60 kPa H_2, 8 kPa H_2O, and balance He) in order to eliminate the effect of deactivation in the kinetic measurements.

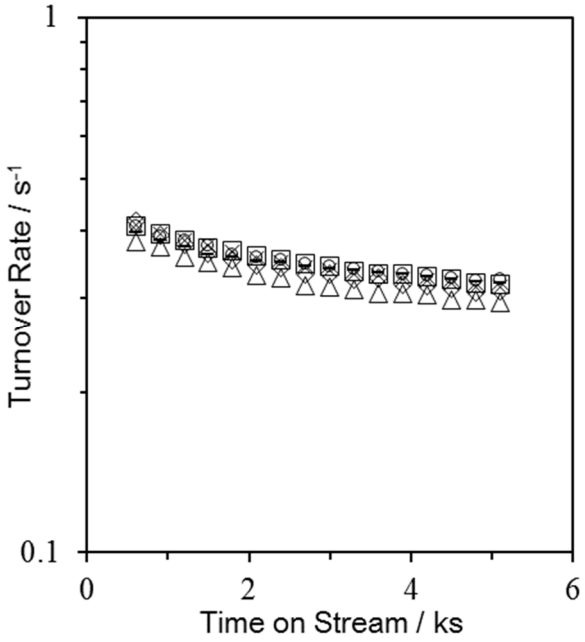

Figure S1. CO hydrogenation turnover rates at steady state condition on catalysts with different intraparticle and interparticle dilutions. (5% wt. Ru/SiO_2, 7.5 nm clusters; 573 K, 2 kPa CO, 60 kPa H_2, 8 kPa H_2O, balance He; the intraparticle and interparticle dilution mass ratios are (□) 1:5 + 1:50, (◊)1:10 + 1:50, (○)1:25 + 1:50, (—)1:50 + 1:50, (Δ)1:10 + 1:20, and (×)1:10 + 1:100, respectively).

S2. Density functional theory models

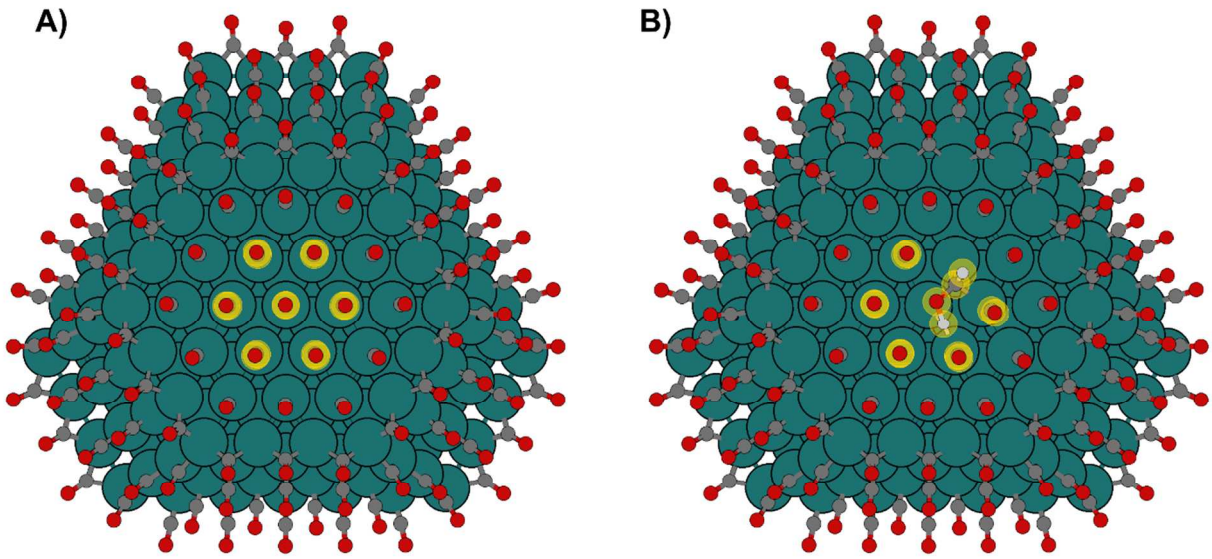

Figure S2. Ru_{218} hemispherical models at 1.04 ML with a) CO*–CO* pair and b) the kinetically-relevant [*HCO–H*]≠ transition state. Frequency calculations are performed on the atoms in yellow for these and all other structures in this work.

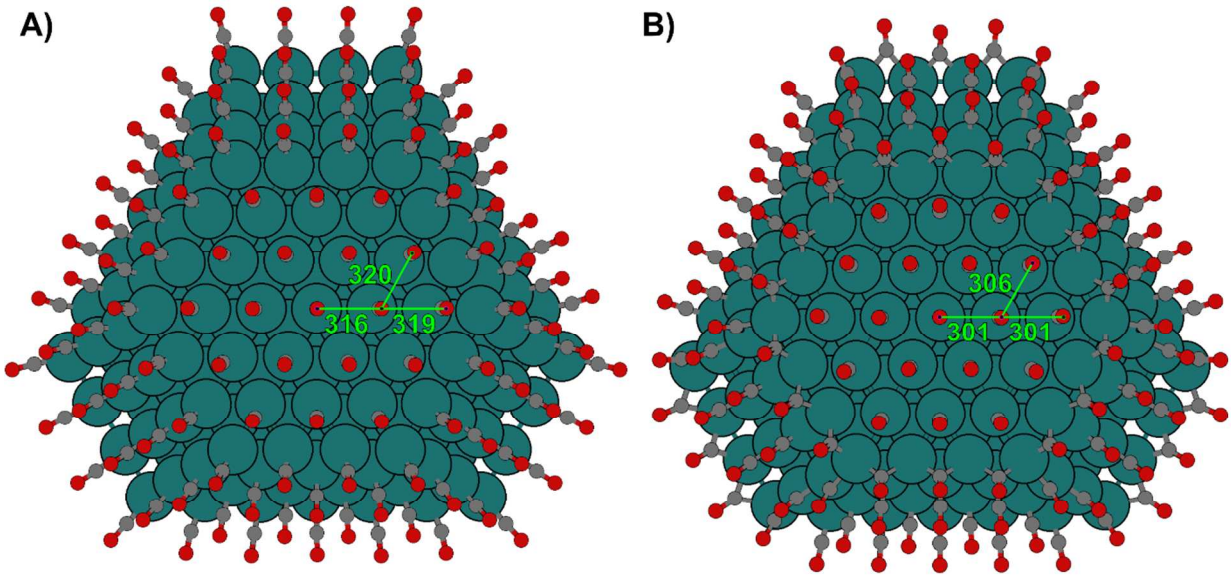

Figure S3. Ru_{218} hemispherical models at a) 1 ML and b) 1.04 ML of CO* with select CO*–CO* inter-adsorbate distances shown in pm.

S3. Details of DFT calculations of thermochemical properties

Frequency calculations were carried out on all optimized states to determine zero-point vibrational energies (*ZPVE*), vibrational enthalpies (H_{vib}), and free energies (G_{vib}). Their values were used, together with VASP-derived electronic energies (E_0), to obtain enthalpies:

$$H = E_0 + ZPVE + H_{vib} + H_{trans} + H_{rot} \tag{S1}$$

and free energies:

$$G = E_0 + ZPVE + G_{vib} + G_{trans} + G_{rot} \tag{S2}$$

for all reactant, product, and transition state structures. For RPBE GGA, the dispersion-corrected enthalpies:

$$H = E_0 + E_d + ZPVE + H_{vib} + H_{trans} + H_{rot} \tag{S3}$$

and free energies:

$$G = E_0 + E_d + ZPVE + G_{vib} + G_{trans} + G_{rot} \tag{S4}$$

Entropy can be determined for a state with a known H and G at a given T:

$$S = \frac{H - G}{T} \tag{S5}$$

For calculations which include the Ru_{218} catalyst model (including adsorbed species and transition states on that surface), there are no translational or rotational degrees of freedom and DFT-derived vibrational frequencies can be used to determine the *ZPVE*, H_{vib} and G_{vib} shown in Equations S6-S8.

$$ZPVE = \sum_i (½ \nu_i h) \tag{S6}$$

$$H_{vib} = \sum_i \left(\frac{\nu_i h e^{\frac{-\nu_i h}{kT}}}{1 - e^{\frac{-\nu_i h}{kT}}} \right) \tag{S7}$$

$$G_{vib} = \sum_i \left(-kT \ln \frac{1}{1 - e^{\frac{-\nu_i h}{kT}}} \right) \tag{S8}$$

where ν_i is the frequency, h is Planck's constant, k is Boltzmann's constant.

Gas-phase molecules have translational and rotational degrees of freedom; thus H_{trans}, H_{rot}, G_{trans} and G_{rot} must also be computed:[1]

$$H_{trans} = {}^5/_2\, kT \tag{S9}$$

$$H_{rot,linear} = kT \tag{S10}$$

$$G_{trans} = -kT \ln \left[\left(\frac{2\pi MkT}{h^2} \right)^{3/2} V \right] \tag{S11}$$

$$G_{rot} = -kT \ln \left[\frac{\pi^{1/2}}{\sigma} \left(\frac{T^3}{\theta_x \theta_y \theta_z} \right)^{1/2} \right] \tag{S12}$$

$$\theta_i = \frac{h^2}{8\pi^2 I_i k} \tag{S13}$$

where I_i is the moment of inertia about axes x, y or z and σ is the symmetry number of the molecule, 2 for H_2, 1 for CO, 2 for H_2O.

S4. In situ FTIR measurements during CO hydrogenation on Ru clusters

The reactivity of various surface CO* species on 5% wt. Ru/SiO_2 were determined by monitoring the changes of corresponding CO* intensities during the reaction of H_2 with chemisorbed CO* in transient FTIR experiments at 418K. Sample pallet was cooled to 418 K after the pre-treatment in flow H_2/He mixture with 50% H_2 (Praxair, 99.999%, 1.67 $cm^3\, g^{-1}\, s^{-1}$) at 723 K (0.033 K s^{-1}) for 2 h.

CO, H_2, and He were introduced together into the cell to reach steady-state condition (0–40 min, Fig. S4) and form chemisorbed CO* adlayers on the surface. CO and H_2 reactant flows were then stopped, and gas-phase CO and H_2—as well as weakly bound CO* and H_2*—were removed in flowing He (40–60 min, Fig. S4). H_2 was then reintroduced to react with the remaining chemisorbed CO* species (60–120 min, Fig. S4). The infrared spectra were recorded continuously and the concentration of various reactants and products were concurrently measured by GC during this process.

Figure S4 shows the evolution of infrared spectra during these transient experiments. CO + H_2 gas flows are stopped at t = 40 min, allowing the inert He flow to remove any weakly bound CO* from the surface. The intensities of all three chemisorbed CO* bands decrease at similar rates under He flow (Fig. S4a), and their total intensity (I_{sum}) decreases by ~ 25% during the 20 min of flow under inert He (Fig. S4b, right y-axis). This indicates that CO* desorption is kinetically-limited at coverages near 0.75 ML, which reflects strongly exothermic CO* adsorption at sub-monolayer coverages, but does not preclude quasi-equilibrated CO* adsorption/desorption at reaction conditions (in which CO* coverages are >0.75 ML and at higher temperatures, >518 K). CH_4 production immediately stops in the absence of H_2 (Fig. S4b, left y-axis, t = 40 min), indicating that all surface-bound H* species rapidly recombine to form H_2 (which is swept away by the inert He flow), this suggests dissociative H_2 chemisorption is quasi-equilibrated at these conditions. CO_2 formation, in contrast, continues in the absence of H_2, although it's rate decreases by a factor of 10 during this inert He flow (Fig. S4b, left y-axis, t = 40–60 min), indicating that CO_2 is formed from the reaction of CO* with a surface-bound intermediate which is slowly removed in the absence of H_2 or H_2O (e.g., O*) rather than with CO* which maintains coverages ≥ 0.75 ML throughout this period. H_2 is re-introduced at t = 60 min, and CH_4 formation occurs immediately and proceeds at rates 10 times faster than at steady state values while CO_2 formation remains undetectable (Fig. S4b, left y-axis, t = 60–120 min), suggesting that CH_4 formation is enhanced by low CO* coverages while CO_2 formation apparently requires near-saturation coverages of CO*. The intensities of all three chemisorbed CO* bands decrease in flowing He/H_2 (Fig. S4a), suggesting all

chemisorbed CO* are reactive and justifying the use of the sum of all bands to quantify chemisorbed CO* at different conditions.

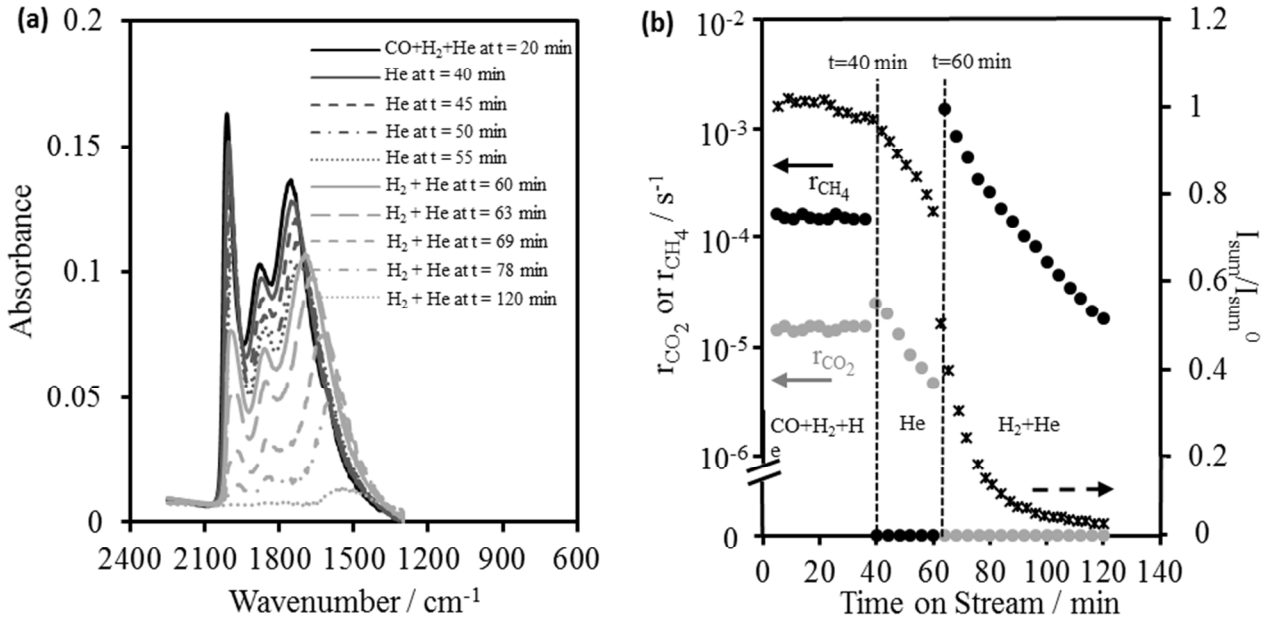

Figure S4. Evolutions of (a) infrared spectra in the C–O stretching region and (b) CH_4 and CO_2 formation rates (left y-axis) and relative total intensity of CO* bands (right y-axis) over time during the transient IR experiments (I_{sum} refers to the total intensity of CO* at specific time and I_{sum}^0 refers to the total intensity of CO* during the steady-state reaction).

S5. Effects of H_2 and H_2O pressures on CO coverages*

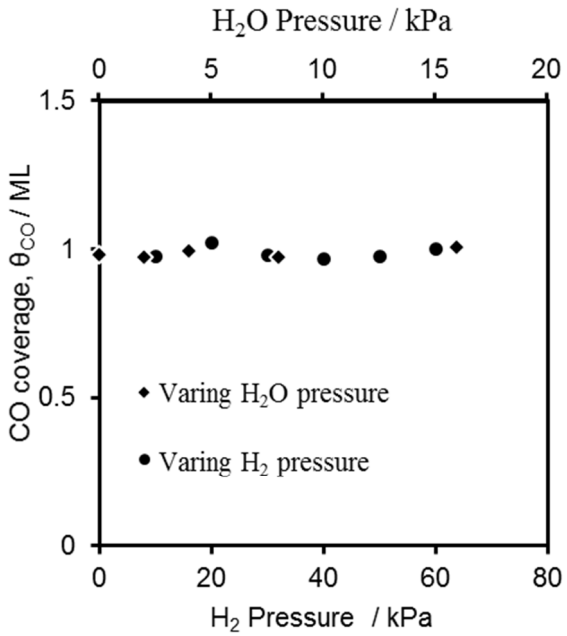

Figure S5. Effects of H_2 (2 kPa CO, 2 kPa H_2O, balance He) and H_2O (2 kPa CO, 2 kPa H_2, balance He) pressures on CO* coverage on 5% wt. Ru/SiO_2 (7.5 nm Ru particle size, 1:10 intraparticle dilution) during CO hydrogenation reaction at 573 K.

S6. Effects of reactant concentrations on CO hydrogenation turnover rates at different temperatures

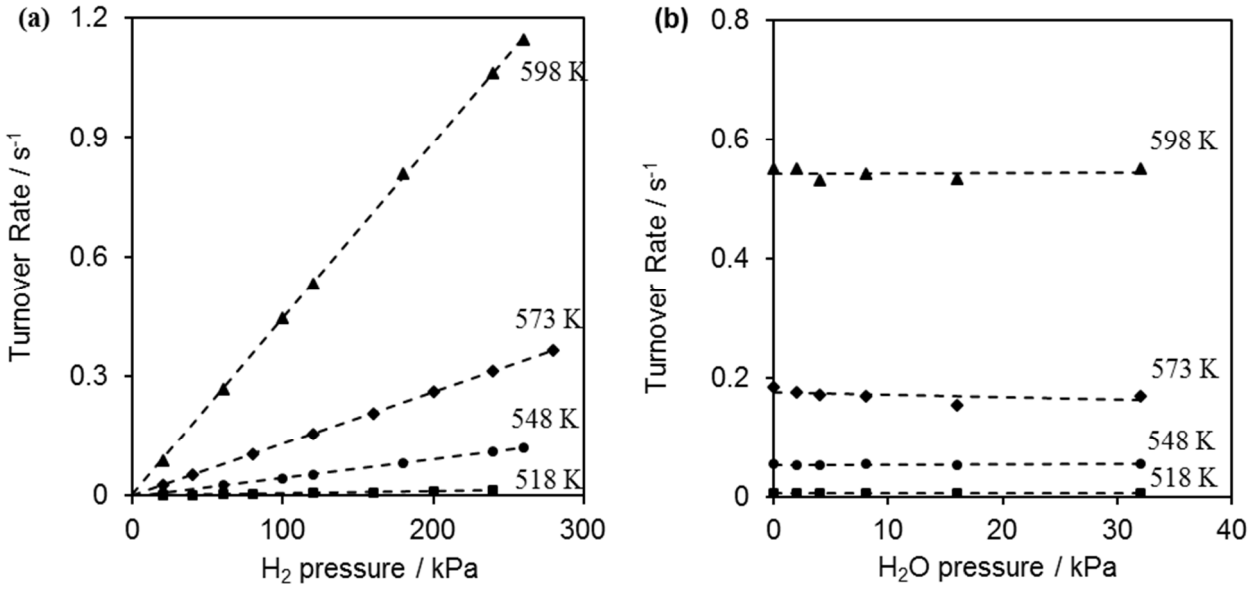

Figure S6. Effect of (a) H_2 (2–280 kPa H_2, 16 kPa CO, 16 kPa H_2O, balance He) and (b) H_2O (0–32 kPa H_2O, 16 kPa CO, 120 kPa H_2, balance He) partial pressures on CO hydrogenation turnover rates on 5% wt. Ru/SiO_2 (7.5 nm particle size, 1:10 intraparticle dilution) at different temperatures.

S7. Derivation of rate equation for CO hydrogenation turnover rate via H-assisted CO activation route

Measured CO hydrogenation turnover rates can be accurately described by Langmuir-Hinshelwood based rate equation (Equation 1 in manuscript) at sub-monolayer CO* coverages (see Figure 6a in manuscript). Equation 1 (in manuscript) can be derived from the elementary steps via H-assisted CO activation route (Steps 1-6 in Scheme 1, in manuscript). Here we describe in detail the derivation of Equation 1 (in manuscript) from the elementary steps in Scheme 1 (in manuscript).

$$[CO^*] = K_{CO}P_{CO}[*] \quad \text{(S14)}$$

$$[H^*] = K_{H_2}^{1/2}P_{H_2}^{1/2}[*] \quad \text{(S15)}$$

$$[HCO^*] = \frac{K_{CO^*-H^*}[CO^*][H^*]}{[*]} = K_{CO^*-H^*}K_{CO}K_{H_2}^{1/2}P_{H_2}^{1/2}P_{CO}[*] \quad \text{(S16)}$$

Step 4 (Scheme 1 in manuscript) as the rate-limiting step:

$$r_{CO-1} = k_{HCO^*-H^*}[HCO^*][H^*] = k_{HCO^*-H^*}K_{CO^*-H^*}K_{CO}K_{H_2}P_{H_2}P_{CO}[*]^2$$

(S17)

Step 5 (Scheme 1 in manuscript) as the rate-limiting step:

$$[HC^*OH^*] = K_{HCO^*-H^*}[HCO^*][H^*] = K_{HCO^*-H^*}K_{CO^*-H^*}K_{CO}K_{H_2}P_{H_2}P_{CO}[*]^2$$

(S18)

$$r_{CO-2} = k_{^*HCOH^*}[^*HCOH^*] = k_{^*HCOH^*}K_{HCO^*-H^*}K_{CO^*-H^*}K_{CO}K_{H_2}P_{H_2}P_{CO}[*]^2$$

(S19)

where $K_{HCO^*-H^*}$ is the equilibrium rate constant for Step 4 when Step 5 is regarded as the rate-limiting step.

The adsorbed CO* and * are the most abundant surface intermediates (MASI) on Ru clusters with sub-monolayer CO* coverages, as suggested from the FTIR results in Figure S5. Therefore, the site balance on surface is:

$$[CO^*] + [*] = K_{CO}P_{CO}[*] + [*] = (K_{CO}P_{CO} + 1)[*] = [L]$$

(S20)

$$\frac{[*]}{[L]} = \frac{1}{1+K_{CO}P_{CO}}$$

(S21)

resulting in the following CO hydrogenation turnover rate equation via H-assisted CO activation route:

Step 4 (Scheme 1 in manuscript) as rate-limiting step:

$$r_{CO-1} = k_{HCO^*-H^*}[HCO^*][H^*] = \frac{k_{HCO^*-H^*}K_{CO^*-H^*}K_{CO}K_{H_2}P_{H_2}P_{CO}}{(1+K_{CO}P_{CO})^2} = \frac{\alpha_1 P_{H_2}P_{CO}}{(1+K_{CO}P_{CO})^2}$$

(S22)

Step 5 (Scheme 1 in manuscript) as rate-limiting step:

$$r_{CO-2} = k_{*HCOH^*}[HC^*OH^*] = \frac{k_{*HCOH^*}K_{HCO^*-H^*}K_{CO^*-H^*}K_{CO}K_{H_2}P_{H_2}P_{CO}}{(1+K_{CO}P_{CO})^2} = \frac{\alpha_2 P_{H_2}P_{CO}}{(1+K_{CO}P_{CO})^2}$$

(S23)

The reversibility of Step 4 (*HCOH* formation) is not kinetically-detectable as either Step 4 or Step 5 in Scheme 1 can be treated as the kinetically-relevant step and would lead to the same functional form of Equation 1, as shown from the above derivations.

S8. Derivation of the effects of activation areas on enhancement factors

Equation 14 (in manuscript) and the high-coverage form of Equation 1 (Eq. 8, in manuscript) depend similarly on H_2 and CO pressures, but, in the case of Equation 14, with an apparent rate constant (k_{app}) given by:

$$k_{app} = \frac{k_B T}{h}\frac{K\neq}{K_{CO}^2}\frac{\gamma_{CO^*}^2}{\gamma_{\neq}} \tag{S24}$$

This apparent rate constant depends on CO* coverage through the $\frac{\gamma_{CO^*}^2}{\gamma_{\neq}}$ term, which reflects the co-adsorbate interactions within the CO* adlayer as it densifies with increasing CO pressure. The enhancement factor (η, Eq. 9, in manuscript) then becomes:

$$\eta = \frac{k_{app}}{k_{ideal}} = \frac{\gamma_{CO^*}^2}{\gamma_{\neq}} \tag{S25}$$

The effect of CO pressure on η is given by:

$$\left(\frac{\partial ln(\eta)}{\partial P_{CO}}\right)_T = \left(\frac{\partial ln(\eta)}{\partial \tau}\right)_T \left(\frac{\partial \tau}{\partial P_{CO}}\right)_T \tag{S26}$$

where τ represents the surface pressure (force per distance) exerted by adsorbed CO* on co-adsorbed species.[131] The surface pressure is analogous to the three-dimensional pressure used to account for similar forces on reaction volumes for homogenous systems.[27-33,131] Such surface pressures must increase monotonically with increasing CO* coverages and thus with CO pressure ($\left(\frac{\partial \tau}{\partial P_{CO}}\right)_T > 0$). The change in enhancement factor (η) with CO pressure can be rewritten in terms of the effects of surface pressure (τ) on both activity coefficients for CO* and the transition state:

$$\left(\frac{\partial ln(\eta)}{\partial P_{CO}}\right)_T = \left[2\left(\frac{\partial ln(\gamma_{CO^*})}{\partial \tau}\right)_T - \left(\frac{\partial ln(\gamma_{\neq})}{\partial \tau}\right)_T\right]\left(\frac{\partial \tau}{\partial P_{CO}}\right)_T \quad \text{(S27)}$$

Both activity coefficients can be described as a function of surface pressure by analogy with treatments for three-dimensional fluid phases:[27-33,131]

$$\gamma_{CO^*} = exp\left(\int_{\tau^0}^{\tau} \frac{(A^0_{CO^*} + \Delta A_{CO^*})d\tau}{RT}\right) \quad \text{(S28)}$$

$$\gamma_{\neq} = exp\left(\int_{\tau^0}^{\tau} \frac{(A^0_{\neq} + \Delta A_{\neq})d\tau}{RT}\right) \quad \text{(S29)}$$

where τ^0 represents the surface pressure at coverages that lead to negligible CO*–CO* interactions (the ideal limit); A^0_{CO*} and $A^0_{\neq}$ represent the partial molal areas occupied by chemisorbed CO and the bound transition state on sparsely-covered (ideal) surfaces; ΔA_{CO*} and $\Delta A_{\neq}$ represent the changes in area that occur as the surface pressure changes from τ^0 to any value τ. Taking the derivatives of Equations S28 and S29 leads to:

$$\left(\frac{\partial ln(\gamma_{CO^*})}{\partial \tau}\right)_T = \frac{A^0_{CO^*} + \Delta A_{CO^*}}{RT} \quad \text{(S30)}$$

$$\left(\frac{\partial ln(\gamma_{\neq})}{\partial \tau}\right)_T = \frac{A^0_{\neq} + \Delta A_{\neq}}{RT} \quad \text{(S31)}$$

which can be substituted into Equation S27 to give:

$$\left(\frac{\partial ln(\eta)}{\partial P_{CO}}\right)_T = \left[\frac{2A^0_{CO^*} - A^0_{\neq}}{RT} + \frac{2\Delta A_{CO^*} - \Delta A_{\neq}}{RT}\right] \cdot \left(\frac{\partial \tau}{\partial P_{CO}}\right)_T \quad \text{(S32)}$$

The difference in area between the transition state ([*HCO–H*]$^{\neq}$) and two CO* molecules can then be considered to be an activation area (ΔA_{act}) for Equation 10 (in manuscript):

$$\Delta A_{act} = A_{\neq} - 2A_{CO^*} \quad \text{(S33)}$$

This activation area is the rigorous analog of the activation volume used to describe the effects of pressure on the dynamics of reactions occurring in a liquid or in non-ideal gaseous media.[27-33,131] The difference in compressibility between the transition state and CO* is given by:

$$\left(\frac{\partial \Delta A_{act}}{\partial \tau}\right)_T = \left(\frac{\partial A_{\neq}}{\partial \tau}\right)_T - 2\left(\frac{\partial A_{CO^*}}{\partial \tau}\right)_T \quad \text{(S34)}$$

Equations S33 and S34 can be substituted into Equation S32 to give an expression for the change in the enhancement factor (η, Eq. S25) as CO pressure increases in terms of an activation area (ΔA_{act}) and how that area varies with surface pressure $\left(\frac{\partial \Delta A_{act}}{\partial \tau}\right)_T$ as the adlayer densifies:

$$\left(\frac{\partial ln(\eta)}{\partial P_{CO}}\right)_T = -\left[\frac{\Delta A^0_{act} + \Delta\Delta A_{act}}{RT}\right] \cdot \left(\frac{\partial \tau}{\partial P_{CO}}\right)_T \quad \text{(S35)}$$

as CO pressure increases. The term in square brackets in Equation S35 (same as Equation 18 in the manuscript) represents the activation area at a specific surface pressure, and its sign determines whether η increases or decreases as adlayers densify, in the same manner as activation volumes determine how hydrostatic pressure influences rates for liquid-phase reactions.[27-33,131]

References

[1] Statistical Mechanics", D. A. McQuarrie, 2000, University Science Books, Sausolito, CA.